Langmuir Article

pubs.acs.org/Langmuir

Interplay between the Transport of Solutes Across Nanofiltration Membranes and the Thermal Properties of the Thin Active Layer

Hafedh Saidani,[†,‡] Nihel Ben Amar,[†] John Palmeri,[§] and André Deratani*[,‡]

[†]*Laboratoire de Modélisation Mathématique et Numérique dans les Sciences de l'Ingénieur, ENIT, Campus Universitaire, B.P 37 Le Belvédère 1002, Tunis, Tunisia,* [‡]*Institut Européen des Membranes, Université Montpellier 2 (ENSCM, UM2, CNRS), 34095 Montpellier Cedex 05, France, and* [§]*Laboratoire de Physique Théorique, UMR CNRS-Université Paul Sabatier, 31062 Toulouse, France*

Received August 4, 2009. Revised Manuscript Received September 15, 2009

The thin active layer (TAL) of seven nanofiltration (NF) membranes was studied using differential scanning calorimetry, and the membranes were classified into two groups according to the polymer physical state (amorphous or semicrystalline). NF membrane performance in terms of permeate volume flux density and rejection of neutral solutes was investigated in temperature cycles. The modeling of rejection using a hindered transport theory showed irreversible and opposite pore size changes for the two groups of NF membranes when the maximum operating temperature of the cycle exceeded the glass-transition temperature of the TAL. A mechanism of pore deformation is proposed to explain the variation of the solute transport properties as a function of the temperature and the polymer physical state in the TAL.

Introduction

Nanofiltration (NF) is an increasingly popular technique for water and waste water treatment for partial desalination, purification, and recovery of valuable compounds.[1−3] In many industrial applications, operating conditions can require elevated working temperatures of ⩾60 °C.[4−6] Membrane manufacturers usually provide the maximum temperature where the NF membranes they produce can be used. However, the performance is indicated in terms of flux and rejection, only with respect to reference temperatures (20 or 25 °C).[7] Therefore, more information in understanding membrane transport properties as a function of temperature is a necessary requirement for practical applications.

Commercial thin film composite NF membranes usually consist of three layers: a polypropylene or polyester nonwoven backing, a microporous polysulphone (PS) support, and a proprietary thin active layer (TAL).[8] In most cases, TAL is fabricated by interfacial polymerization to give a polyamide (PA) top layer.[9,10] TAL is cross-linked to induce porosity and stabilize the structure. Although TAL is cross-linked, we have recently reported that working at temperatures higher than room temperature could lead to changes in the membrane morphology, especially affecting physical characteristics such as the effective thickness and pore radius (DESAL DK membrane GE Osmonics).[11]

The effect of temperature on the performances of the NF polymeric membrane has only recently attracted attention. In term of flux, all of the studies showed an increase in membrane permeability by increasing the operating temperature.[11−14] This behavior has been previously attributed to the decrease in solution viscosity. Actually, we showed that the bulk-viscosity-corrected permeability cannot completely explain the increase in permeability with temperature and that a complete description needs to take into account morphological membrane changes as mentioned above.[11] Another striking phenomenon is that the pure water permeability measurement at a given temperature is not reproducible after temperature cycling, giving rise to hysteresis. Thus, water permeability is significantly reduced after temperature cycling in the range of 20−50 °C in the case of the NFT-50 membrane[15] and 25−65 °C in the case of the XN-40 membrane and, to a lesser extent, the TS-80 membrane.[4] In the last case, a critical temperature can be observed somewhere between 55 and 65 °C, below which no hysteresis was found.

In most studies, solute rejection decreased with increasing temperature. The salt rejection was less influenced by temperature than the rejection of neutral solutes.[14] It can be concluded that the electric interactions due to the membrane surface charges are less influenced by temperature than solute diffusion into the pores. This is supported by simplistic theoretical calculations using the Debye screening length and solute diffusion (Stokes−Einstein equation).[15] In addition to the charge effects, membrane structural change can also play an important role in determining the variation of solute retention performance with temperature.[16]

*Corresponding author. E-mail: andre.deratani@iemm.univ-montp2.fr.

(1) Lipnizki, F.; Trägårdh, G. In *Proceedings of 9th World Filtration Congress*, New Orleans, April 2004, 18−22.
(2) Wittman, E. La nanofiltration dans le domaine du traitement des eaux: conditions d'application et modélisation. Ph.D. Thesis, University of Montpellier 2, France, **1998**.
(3) Ventresque, C.; Gisclon, V.; Bablon, G.; Chagneau, G. *Desalination* **2000**, *131*, 1–16.
(4) Manttari, M.; Pihlajamski, A.; Kaipainen, E.; Nyström, M. *Desalination* **2002**, *145*, 81–86.
(5) Chen, C.; Chai, X.; Yue, P.; Mi, Y. *J. Membrane Sci.* **1997**, *127*, 93–99.
(6) Snow, M. J. H.; de Winter, D.; Buckingham, R.; Campbell, J.; Wagner, J. *Desalination* **1996**, *105*, 57–61.
(7) *Desal Pure Water*, Membrane Technology & Applications; GE-Osmonics; 2003.
(8) Petersen, R. J.; Cadotte, J. E. In *Handbook of Industrial Membrane Technology*; Porter, M. E., Ed.; Noyes Publications: Park Ridge, NJ, 1990.
(9) Freger, V.; Srebnik, S. *J. Appl. Polym. Sci.* **2003**, *88*, 1162–1169.
(10) Tang, C. Y.; Kwon, Y.-N.; Leckie, J. O. *Desalination* **2009**, *242*, 149–167.
(11) Ben Amar, N.; Saidani, H.; Deratani, A.; Palmeri, A. *Langmuir* **2007**, *23*, 2937–2952.
(12) Schaep, J.; Van der Bruggen, B.; Uytterhoeven, S.; Croux, R.; Vandecasteele, C.; Wilms, D.; Van Houtte, E.; Vanlerberghe, F. *Desalination* **1998**, *119*, 295–302.
(13) Nilsson, M.; Tragardh, G.; Ostergren, K. *J. Membrane Sci.* **2008**, *312*, 97–106.
(14) Sharma, R. R.; Chellam, S. *J. Colloid Interface Sci.* **2006**, *298*, 327–340.
(15) Nilsson, M.; Trägårdh, G.; Ostergren, K. *J. Membrane Sci.* **2006**, *280*, 928–936.
(16) Yao, X.; Kennedy, K. J.; Tam, C. M.; Hazlett, J. D. *Can. J. Chem. Eng.* **1994**, *72*, 991–999.

Table 1. Properties of the Studied Membranes

	manufacturer data				experimental data	
membrane	manufacturer	thin film layer	maximum temperature (°C)	maximum pressure (bar)	MWCO (Da, 30°C)	permeability (L/h·m^2·bar, 30°C)
DESAL DL	GE Osmonics	cross-linked aromatic polyamide	55	41	327[b]	12.6[e]
DESAL DK					225[e]	9.1[e]
NF	Dow Filmtec	polyamide	45	40	300[a]	10.5[a]
NF90					200[e]	9.5[e]
NF200					360[c]	11.5[a]
NF270					300[e]	18.9[d]
NFT-50	Alfa Laval	aromatic/aliphatic polyamide	50	55	150[b]	9.0[b]

[a] From ref 20. [b] From ref 21. [c] From ref 22. [d] From ref 23. [e] This study.

Yao et al. suggested that high temperature may permanently reorient the polymer chains in an open membrane because of its less dense polymer structure compared to that of a tight membrane.[16] According to Nilsson et al., this temperature-induced hysteresis in performance may originate from the temperature-induced relaxation of the polymer matrix.[13] From these authors, both steric and electrostatic forces influence the relaxation of the swollen structure during rinsing with pure water. The steric force is assumed to be due to the restriction of macromolecule mobility because the polymer chains act as wedges against each other. At higher temperatures, the mobility of the polymer chains increases, giving rise to additional polymer relaxation, which could explain the observed hysteresis in permeability after temperature cycling. If relaxation takes place at a higher temperature, then it could result in a structure that appears to be kinetically frozen at lower temperatures.

Actually, no further study yielded physical proof to ascertain the previously reported assumptions. Although they seem to be consistent, more information about the polymer thermal properties in the TAL should give insight into the mechanism inducing the structural change expected to occur during high-temperature cycling. As mentioned before, different authors in the literature concluded that the operating conditions for NF should be restricted to the small-temperature domain (usually $T < 50$ °C) in which polymeric membrane performance is reproducible. Understanding this point therefore appears to be of the greatest importance from a practical point of view to enlarge the potential NF applications at higher temperatures to those involved in many industries.

In this study, the thermal behavior of TAL was investigated using differential scanning calorimetry for seven commercially available polymeric NF membranes. This was done after removing the TAL from the membrane in order to make sure that the properties analyzed were characteristic of the top layer. Besides, these studied membranes were characterized in terms of pure water permeability and neutral solute rejection as a function of temperature cycling. From these experiments, the pore size variation was estimated using the Nanoflux NF modeling software.[17,18] Finally, a mechanism explaining the variation of membrane performance is proposed that takes into account the polymer deformation with temperature cycling.

Experimental Section

Setup and Permeation Procedure. *Membranes, Feed, and Solutes*. Seven commercially available NF membranes from GE Osmonics (Fairfield, CT), Dow Filmtech (Midland, MI), and Alfa Laval (Les Clayes-sous-Bois, France) were used in this study. All of them are thin film composite membranes consisting of three layers: an ultrathin top surface layer (TAL) deposited onto a porous PS interlayer, itself supported on a nonwoven fabric conferring to the composite good mechanical properties. Table 1 presents some characteristics of the studied membranes given by the manufacturers, including the molecular weight cutoff (MWCO) and pure water permeability data determined under similar operating conditions (flat sheet, 30 °C).

Table 2. Properties of the Studied Neutral Solutes

solute	molecular weight (kg/kmol)	diffusivity (m^2/s) at 25 °C	Stokes radii (nm)
ethylene glycol	62	1.15×10^{-9}[a]	0.212
glycerol	92	0.94×10^{-9}[b]	0.260
triethylene glycol	150	0.76×10^{-10}[a]	0.320
arabinose	150	0.76×10^{-9}[b]	0.323
glucose	180	0.67×10^{-9}[b]	0.365

[a] From ref 19. [b] From ref 11.

Two kinds of feed solutions were nanofiltered: pure water and uncharged solute solutions to determine the impact of temperature variation on both the permeation rate and the pore size. Deionized water (5 MΩ·cm) (RIOS 8, Millipore Corp.) was used for the preparation of feed solutions. The rejection experiments were carried out using the neutral solutes listed in Table 2 along with their properties. These compounds were chosen because it is believed that they present weak binding interactions with membranes owing to their hydrophilic chemical nature. The Stokes radii were determined from their bulk diffusivity using the Stokes−Einstein equation.[19] A low feed concentration (1 g/L) was used for all of the solution compounds to limit the solute−solute interaction. The solute concentrations were determined using an interferometer refractometer (Optilab DSP, Wyatt Technology).

Permeation Setup. The membranes were placed inside a Sepa CF II laboratory-scale 316 SS cell system (GE Osmonics), which was loaded with a 0.79 mm (31 mil) rectangular spacer (14 cm × 9 cm, 133 cm^2), providing a total feed side channel depth of 0.84 mm (33 mil). The feed solution was delivered by a volumetric pump (Cat pump 231) at a constant flow of 9 L/min from a 32 L feed tank. The temperature in the feed tank was controlled using an immersed stainless steel coil with a liquid circulated from a temperature regulation system (Frigitherm-10 P-Selecta). The closed loop of the feed solution was made of high-temperature, pressure-resistant tubing (up to 60 °C and 20 bar). The feed solution was circulated at a constant tangential velocity (1.23 m/s),

(17) Palmeri, J.; Sandeaux, J.; Sandeaux, R.; Lefebvre, X.; David, P.; Guizard, C.; Amblard, P.; Diaz, J. F.; Lamaze, B. *Desalination* **2002**, *147*, 231–236.
(18) Lefebvre, X.; Palmeri, J.; Sandeaux, J.; Sandeaux, R.; David, P.; Maleyre, B.; Guizard, C.; Amblard, P.; Diaz, J. F; Lamaze, B. *Sep. Purif. Technol.* **2003**, *32*, 117–126.
(19) Paduano, L.; Sartorio, R.; D'Errico, G.; Vitagliano, V. *J. Chem. Soc., Faraday Trans.* **1998**, *94*, 2571–2576.
(20) Zhu, A.; Long, F.; Wang, X.; Zhu, W.; Ma, J. *Chemosphere* **2007**, *67*, 1558–1565.
(21) Cavaco Morão, A. I.; Brites Alves, A. M.; Costa, M. C.; Cardoso, J. P. *Chem. Eng. Sci.* **2006**, *61*, 2418–2427.
(22) Namguk, H.; Gary, A.; Hyoung-Ryun, P.; Myoungsuk, S. *Water Res.* **2004**, *38*, 1427–1438.
(23) Lin, Y. L.; Chiang, P. C.; Chang, E. E. *J. Hazard. Mater.* **2007**, *146*, 20–29.

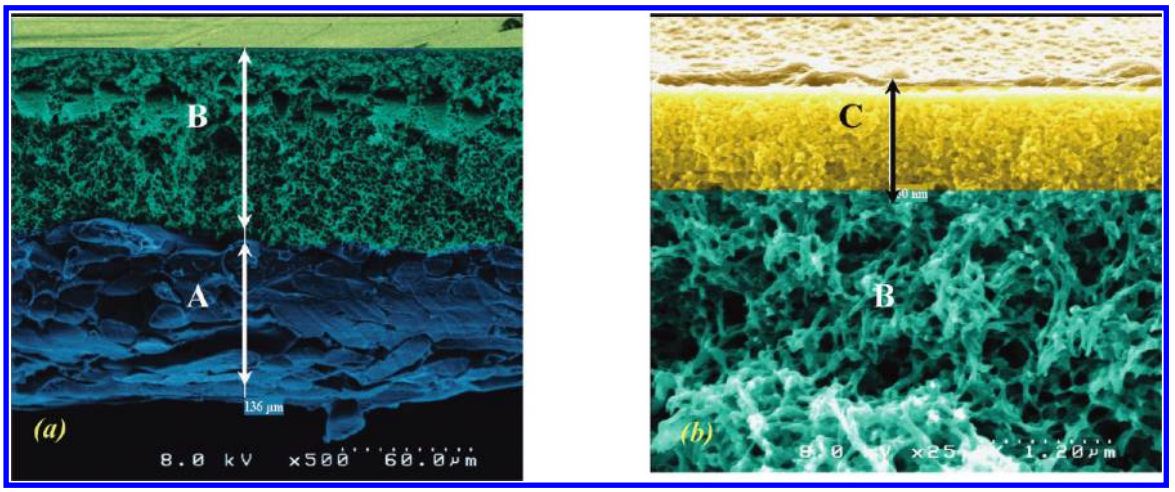

Figure 1. SEM observation of the NF membrane cross-section (DK membrane): Magnification (a) ×500 and (b) ×20 000. Layers A−C stand for the woven fabric, the microporous support, and the TAL, respectively.

which allows us to neglect concentration polarization effects (consistent with the monotonically increasing rejection vs flux curves observed experimentally). The greatest permeate recovery calculated is 0.7%, a value that validates our assumption of constant feed tank concentration even before manually reintroducing the permeate sample into the tank. The membrane volume permeation rate was determined by weight (Sartorius CP323S), and the data obtained were corrected by the density at the studied temperature. More details can be found elsewhere.[11]

Permeation Procedure. Prior to use, the membranes were washed for 2 h at 40 °C under pressure (20 bar) with pure water to remove chemical preservation products and to avoid compaction and temperature effects in further tests. The washing pressure was chosen to be greater than the maximum pressure used in permeation and rejection experiments (15 bar) and lower than the maximum pressure recommended by the manufacturer (Table 1). Then, a circulation of 1 g/L propylene glycol solution was performed for 4 h at low pressure (2 bar). Starting from this value, we progressively increased the pressure in steps of 2 bar every 5 min until reaching the maximum pressure of 15 bar. We then proceeded to a membrane rinsing step with pure water for 1 h at 10 bar and ambient temperature. This protocol assures us of attaining the steady-state characteristics of the membrane.

For all of the experiments carried out, the temperature effect was studied by increasing or decreasing the temperature. The change in temperature was performed without circulating the feed solution. When the desired temperature was reached, the feed was circulated and the pressure was increased step by step from 5 to 15 bar. A circulation time of 5 min was generally long enough to allow the steady state to be reached. Then, the permeate was weighed for 30 min and recycled back into the feed. Finally, a 5 mL sample was collected for solute concentration analysis.

Membrane Characterization. *Membrane Morphology*. The morphology of the studied membranes was characterized by a cold cathode field emission scanning electron microscope (Hitachi S-4500, resolution of 1.5 nm at 15 kV). Before SEM observation, the samples first had gone through the prewash and pressure compaction procedure. Specimens were then prepared by fracturing the membrane samples in liquid nitrogen and covering them with a thin layer of Pt by sputter coating.

Separation of TAL from the Support Layers. NF membranes are composite materials (Figure 1). The top-surface selective barrier layer (Figure 1 C) was separated from the other two layers (Figure 1A,B) to determine its intrinsic thermal properties. The following protocol adapted from a previously described procedure was applied.[24,25] The membrane was placed on a glass plate upside down and soaked with a mixture of 50/50 v/v toluene/propanol-2 so that the sample stuck on the glass plate after drying. The PS layer was then dissolved by soaking the membrane in dimethyl formamide (DMF) and drying in air for 15 min. The procedure was repeated twice. The resulting membrane was then rinsed twice with dichloromethane (DCM) and allowed to dry overnight. Afterwards, the nonwoven fabric could easily be peeled off. Then, the remaining PA layer was again soaked in DMF until the membrane became fully transparent, indicating that the PS layer was no longer present, and was then washed with DCM as described above. After drying, the PA polyamide layer was scratched off the glass plate as lumps for DSC analysis.

Transition-Temperature Determination. The temperature of phase transitions occurring in the membrane materials was determined using differential scanning calorimetry (DSC) (TA Instrument DSC2920). Measurements were carried out at a 10 °C/min heating/cooling rate. The membrane sample (10 mg) was arranged upside down to allow the top surface layer to be in contact with the bottom of the crucible. The TAL sample (10 mg) was cut into small pieces of about 1 mm before introducing it into the crucible. After the first heating scan, the DSC data were reproducible in subsequent heating/cooling cycles and the transition temperatures were determined using TA Universal Analysis software. DSC analysis was carried out in the temperature range of −20 to +200 °C and never went beyond the latter temperature to avoid thermal decomposition.

Results and Discussion

Membrane Characterization. In this section, we first present the morphological characterization of the studied NF membranes and then the determination of the TAL thermal properties using the DSC technique.

Membrane Morphology. As shown in the SEM photographs (Figure 1), the studied composite polymer membranes are formed by the superposition of three layers. The bottom layer (A) is a woven fabric on which is deposited a microporous support (layer B) (Figure 1a). An enlarged top view of membranes clearly shows the presence of the TAL (layer C) (Figure 1b).

The total thickness and that of the TAL were determined from the SEM photographs (Table 3). Actually, the TAL thickness is not uniform along the sample. This phenomenon is mainly due to the roughness of the interface between the TAL and the PS support (layer B) and to its more or less high penetration in the latter. That is why the values indicated in Table 3 were obtained by an average of three measures. It should be noted that the thickness was determined from dried membrane samples. A rather large variability in the total thickness was found for the studied membranes, with the thinnest being the NFT-50 (50 μm) and the

Table 3. Thickness Determined by SEM for the Different Layers of the Studied Membranes

membrane	DL	DK	NF	NF90	NF200	NF270	NFT-50
thickness of the top active layer (μm)	0.300	0.700	0.150	0.180	0.200	0.170	0.095
total thickness [A + B + C] (μm)	120	136	110	120	95	65	50

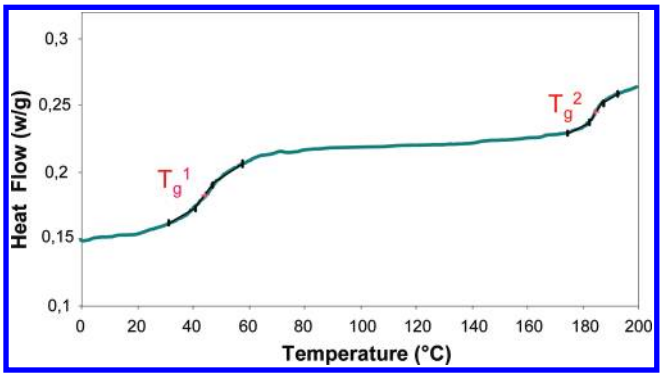

Figure 2. DSC trace for the complete three-layer NF90 membrane.

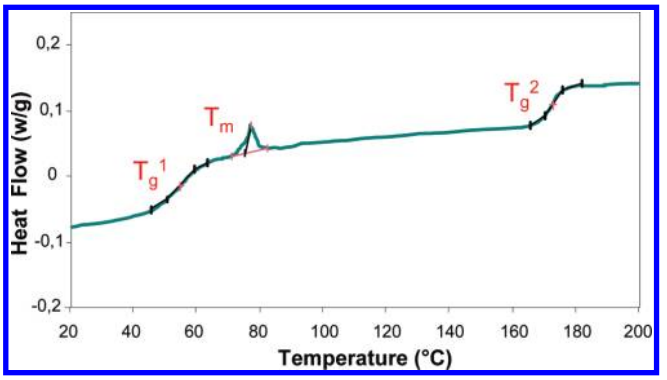

Figure 3. DSC trace for the complete three-layer DK membrane.

thickest being the DESAL DK (136 μm). As seen in Table 3, an even larger variability between these two membranes was observed for the TAL thickness. Measurements indicate that membranes can be classified according to the manufacturer: the thinnest TAL is that of Alfa Laval NFT-50, intermediate values were obtained for Dowfilmtec membranes, and the GE-Osmonics membranes have the greatest TAL thickness. We noticed a certain homogeneity for Dow Filmtech membranes with a value of about 175 nm. In the case of asymmetric membranes, it is usually assumed that the transport resistance is mainly due to the TAL. Unfortunately, a clear relationship between the water permeability for membranes of similar MWCO (Table 1) and our TAL thickness measurements (Table 3) could not be established. For instance, the NF 270 membrane is about twice as permeable as the NF membrane in spite of a similar TAL thickness and MWCO. However, the DK and NF90 membranes have about the same permeability but have very different TAL thicknesses. Interestingly, this suggests that others parameters such as pore tortuosity and interactions between the water solution and membrane material must be taken into account to explain the transport resistance of these materials.

Transition Temperatures. To elucidate the temperature effect on NF membrane performance, we focused on the investigation of their thermal properties using DSC. Obviously, the glass-transition temperature (T_g) and melting point (T_m) of the polymer matrix constituting TAL should have a direct influence on the membrane properties, especially the mechanical stability. T_g, a characteristic parameter of an amorphous polymer phase, is related to the passage from the glassy state to the rubbery state, accompanied by a drastic variation in mechanical properties, such as the Young's modulus, reflecting the material rigidity. Moreover, T_m, a characteristic parameter of the crystalline phase, indicates the passage from a solid phase to a fluid.[26]

The obtained DSC thermograms for the complete three-layer membranes can be classified into two categories: the first group gathers the NF90, NF, NF200, NF270, and NFT50 membranes that present a similar profile showing two second-order transitions T_g (T_g^1 and T_g^2 as displayed for the NF90 membrane in Figure 2) and a second group containing the DK and DL membranes differing by the presence of an additional first-order transition peak assigned to T_m (as displayed for the DK membrane in Figure 3). T_g^1, T_m, and T_g^2 values are in the ranges of 32−57, 80, and 160−185 °C, respectively (Table 4).

Table 4. Glass-Transition Temperature and Melting Point Determined by DSC for the Different Layers of the Studied Membranes

membrane	DL	DK	NF	NF90	NF200	NF270	NFT-50
T_g of the TAL (°C)	53	56	42	43	42	41	32
T_m of the surface layer (°C)	83	79					
T_g of support layer (°C)	174	176	185	180	172	186	160

Although the true chemical natures of the polymers constituting the membranes remain unknown, manufacturers indicate that the TAL of the studied membranes is based on PA, whereas the porous sublayer consists of PS. A recent study has reported that the sulfonated PS generally used in membrane preparation shows T_g in the range of 183−200 °C,[27] which is in good agreement with the T_g^2 values that we observed for the different samples. It was then assumed that T_g^2 might be the fingerprint of the polymer constituting the porous layer. Consequently, T_g^1 is expected to be characteristic of the TAL. It has been reported that the TAL of composite RO and NF membranes is generally composed of either fully aromatic amide or semiaromatic amide groups.[10] Unfortunately, T_g values of aromatic polymers are much higher than the values found in our study, and T_g values between 40 and 60 °C should rather correspond to aliphatic PA.[28,29] In the past decade, numerous studies have shown that a strong decrease in T_g in comparison with the bulk samples can be observed in confined polymer films.[30] For instance, a reduction as large as 70 K has been measured for a polystyrene film with a 29 nm thickness.[31] This situation is also encountered in nanoporous materials in which thin walls of polymer surround the pores.[32]

To confirm our hypothesis, the TAL was separated from the whole membrane by dissolving the PS sublayer in an appropriate solvent according to a procedure previously described.[25,26] The procedure has been proven to change neither the TAL chemical

(24) Freger, V.; Ben-David, A. *Anal. Chem.* **2005**, *77*, 6019–6025.
(25) Freger, V. *Environ. Sci. Technol.* **2000**, *34*, 3710.
(26) Wunderlich, B. *Macromol. Sci., Part B* **2003**, *42*, 579 − 598.
(27) Pedicini, R.; Carbone, A.; Sacca, A.; Gatto, I.; Di Marco, G.; Passalacqua, E. *Polym. Test.* **2008**, *27*, 248–259.
(28) Deimede, V. A. K.; Fragou, V.; Koulouri, E. G.; Kallitsis, J. K.; Voyiatzis, G. A. *Polymer* **2000**, *41*, 9095–9101.

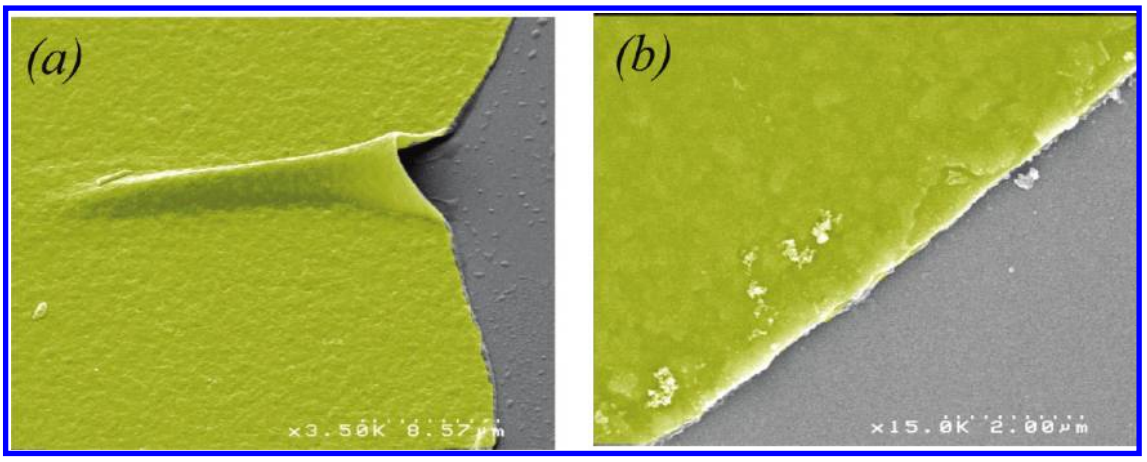

Figure 4. SEM of the isolated TAL from the NF90 membrane. Magnification (a) ×3500 and (b) ×15 000.

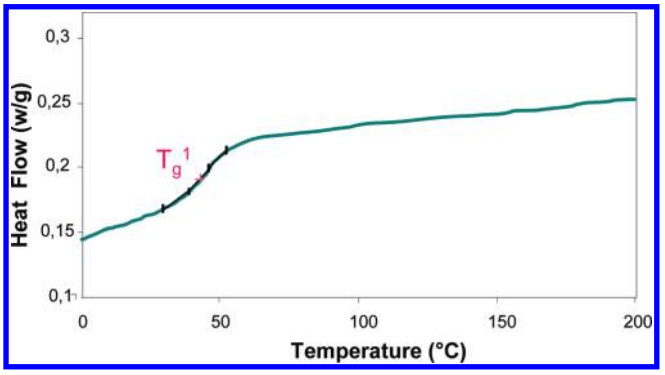

Figure 5. DSC trace for the TAL of the NF90 membrane.

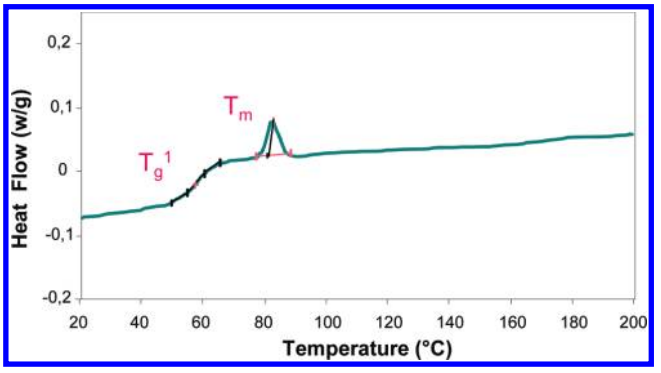

Figure 6. DSC trace for the TAL of the DK membrane.

nature nor its morphology. As an example, Figure 4 shows SEM pictures of the isolated TAL obtained from NF90 membrane. The observed thickness for this sample (0.160 μm) is in excellent agreement with the value determined from the whole membrane (0.180 μm). The separated TAL samples were then subjected to DSC analysis.

The thermogram profile obtained for the NF90 membrane belonging to the first group (Figure 5) now exhibits only the presence of T_g^1. By comparing this result with that obtained for the whole membrane (Figure 3), we concluded that the first transition is representative of the NF90 TAL. In the same way, the thermogram profile of the DK membrane belonging to the second group (Figure 6) presents both T_g^1 and T_m. Again, we can conclude that both of these transitions characterize the thermal properties of the DK TAL. These results validate our assumption that the transition from the glassy to the rubbery state takes place at T_g^1 in the TAL and T_g^2 in the PS sublayer (Table 4). It should be noted that these results also confirm that the procedure used to isolate the TAL does not much alter the polymer thermal properties because very similar transition-temperature values (with a ±2 °C deviation) between the whole membrane and the separated TAL were obtained. Interestingly, the thermal analysis of the second membrane group demonstrates the existence of a melting peak, suggesting that the TAL consists of a semicrystalline polymer in this case. By contrast, the first group does not show such a peak, suggesting that in this case the TAL is made of a completely amorphous polymer.[33,34]

We indeed notice that the TALs of membranes from the same manufacturer have similar thermal behavior (Table 4). The DK and DL membranes from GE-Osmonics in addition to the feature of having a T_m at 80 °C have T_g^1 values higher than 50 °C, whereas the NFT-50 Alfa Laval membrane have a lower value (35 °C) and the Dow FilmTec membranes have an intermediate value (40 °C). This distribution according to the commercial source is believed to be due to the chemical nature of the polymer constituting the TAL.[10,35] However, we believe that the membrane thickness might also play a significant role because thinner layers have lower T_g^1 values.

The maximum operating temperatures recommended by the manufacturers (Table 1) are in good agreement with the measured T_g^1 values (Table 4), suggesting that the upper limit of the temperature domain in using an NF composite membrane is determined by this physical characteristic of the TAL membrane. The question that now can be addressed is to what extent the glass transition affects the performance of NF membranes.

Temperature Effect on the Permeability and Rejection of NF Membranes. In this part, we describe the membrane performance according to the operating temperature in terms of pure water permeability and neutral solute rejection. The experiments were conducted by performing successive cycles in temperature. Two kinds of experiments were designed, characterized by the maximum temperature (T_{max}) reached in each cycle: in the first series, T_{max} was kept at a value lower than T_g^1, whereas in the second series, T_{max} exceeded T_g^1 but remained below T_m. Because we chose NF90 and DK membranes representative of the two NF membrane groups as defined from the thermal properties,

(29) Xijun, L.; Zhaohua, J.; Wenming, Z. *e-Polym.* **2007**, *119*, 1–14.
(30) Dalnoki-Veress, K.; Forrest, J. A.; Murray, C.; Gigault, C.; Dutcher, J. R. *Phys. Rev. E* **2001**, *63*, 031801.
(31) Forrest, J. A.; Dalnoki-Veress, K.; Stevens, J. R.; Dutcher, J. R. *Phys. Rev. Lett.* **1996**, *77*, 2002.

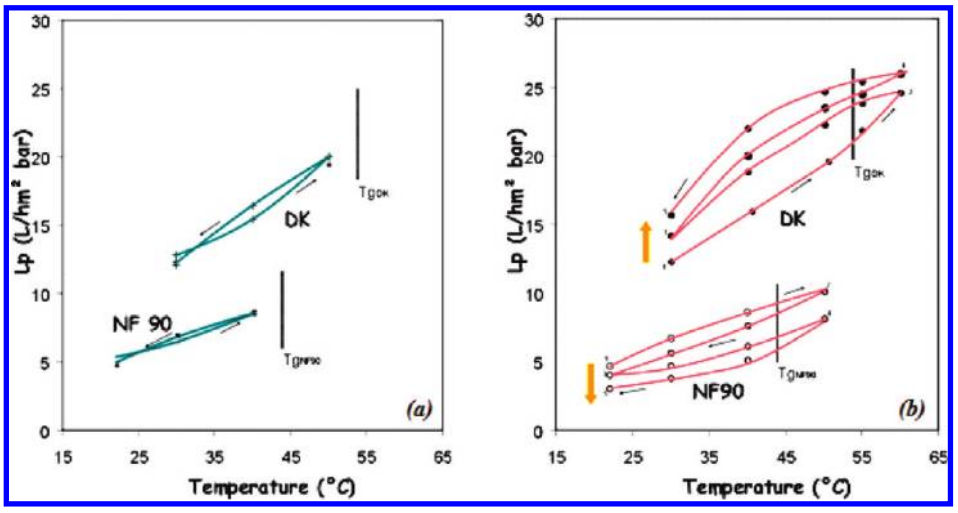

Figure 7. Water permeability of the NF90 and DK membranes in temperature cycle experiments. (a) $T_{max} < T_g^1$ and (b) $T_g^1 < T_{max}$.

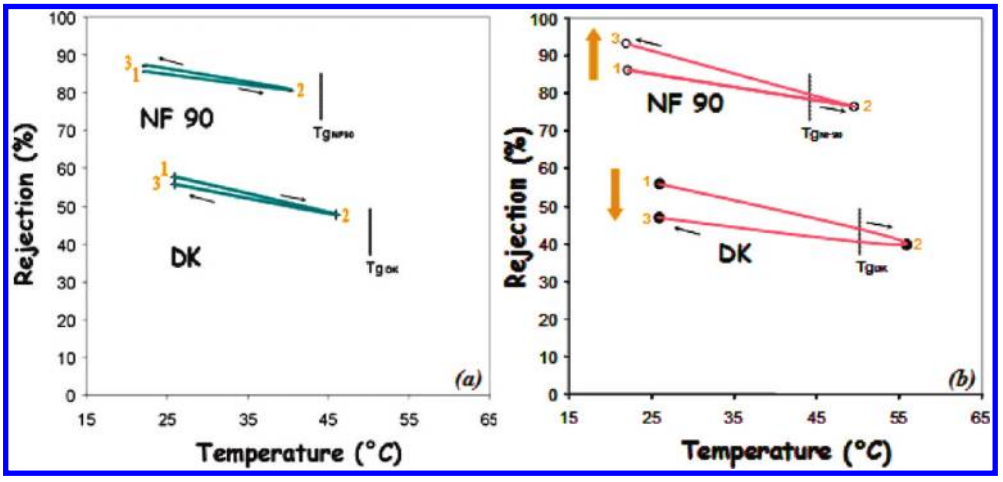

Figure 8. Arabinose rejection (at 13 bar) for the NF90 and DK membranes in temperature cycle experiments. (a) $T_{max} < T_g^1$ and (b) $T_g^1 < T_{max}$.

T_{max} was 40 and 50 °C for the first series of experiments and 50 and 60 °C for the second series.

Pure Water Permeability. The water permeability of the studied NF membranes increases upon increasing the operating temperature (Figure 7). As shown in Figure 7a, the water permeability is quite reproducible during the first series cycles ($T_{max} < T_g^1$) for both membranes because the same value (in the range of experimental errors) is recovered at a given temperature whatever the direction (up and down) of the temperature cycle. The permeability improvement mainly originates from the decrease in viscosity upon increasing temperature, as we have shown in a previous study for the DK membrane.[11] Moreover, it has been shown in this article that the permeability corrected by bulk viscosity cannot completely account for the permeability enhancement observed by increasing the operating temperature. The residual temperature dependence has been assigned to a structural change in the TAL polymer matrix leading to a pore radius increase, as demonstrated by the variation of neutral solute rejection and modeling. (See the next section.)

Conversely, it was found in the second series of experiments ($T_{max} > T_g^1$) that the water permeability evolution as a function of the temperature cycle exhibits hysteresis and could no longer be considered to be reproducible because its value varied according to the thermal history of the membrane sample (Figure 7b). This result indicates that irreversible morphological changes occur when the operating temperature exceeds T_g^1. Surprisingly, two opposite behaviors can be seen for the two studied membranes: whereas the NF90 membrane displays a water permeability declining cycle after cycle (by about 20% per cycle), the water permeability of the DK membrane is enhanced by about 15% per cycle.

A water permeability evolution similar to that observed for the NF90 membrane has been reported in the case of the NFT-50 membrane, belonging to the same group according to our classification from thermal analysis.[12,14] By performing temperature cycles with $T_{max} > 40$ °C, it was found that hysteresis takes place with a significant reduction of the permeability values. For instance, a permeability decline of 20% has been observed after one cycle with $T_{max} = 40$ °C. The authors assumed that the temperature-induced behavior might originate from the swelling of the polymer matrix owing to greater chain mobility at high temperature. The freezing of this relaxed structure during cooling would involve a permeability decline. Although attractive, no physical proof has been provided to support this assumption. Moreover, it remains unclear at this point why the temperature-induced relaxation of the polymer matrix, leading to an enhancement of the flux at high temperature, might yield a flux decline in the frozen state and how this effect might account for the

opposing temperature-induced behaviors such as those observed for the NF90 and DK membranes.

As mentioned above, structural changes in the TAL should result in a modification of rejection performance. Therefore, the next paragraph is devoted to the study of neutral solute rejection as a function of temperature cycles such as those used for the permeation of pure water.

Neutral Solute Rejection. For the sake of clarity, data comparing rejection performance as a function of temperature are presented only in the case of arabinose. This neutral solute is rejected at room temperature at an intermediate value by both the NF90 and DK membranes, as seen in Figure 8a. A temperature increase of the feed solution generally causes a rejection decrease of neutral solutes, which can be explained by an expansion of the polymer network constituting the NF membrane TAL.[11−13] This expected evolution of the arabinose rejection versus temperature was observed whatever the membrane and the operating conditions (Figure 8). The first series of experiments showed that varying the temperature in cycles by keeping T_{max} lower than the corresponding $T_g{}^1$ results in acceptable reproducible membrane performance (Figure 8a). In this range of temperature, we assume that the structural change giving rise to an increase in pore size upon increasing temperature can be considered reversible because the initial membrane performance is recovered after each cycle. Conversely, it was found that the initial membrane performance was not recovered after a temperature cycle when T_{max} was fixed at a value higher than the corresponding $T_g{}^1$ (Figure 8b). Again, two opposite trends were observed; the arabinose rejection is enhanced by using the NF90 membrane, but it is reduced by using the DK membrane. These observations suggest opposite irreversible variations of the pore dimension: in the case of the NF90 membrane, temperature cycling over $T_g{}^1$ would result in a decrease in the pore size radius as revealed by both a rejection increase and a permeability decrease, whereas in the case of the DK membrane both a rejection decrease and a permeability increase would indicate an increase in the pore radius.

Modeling. To quantify the variation of pore size as a function of temperature cycling, we employ a model based on the hindered transport theory that has been developed for hard spheres in cylindrical pores and extended it to more complicated porous structures by introducing a tortuosity correction. The permeation flux can be described by a diffusive term and a convective term. The hindered diffusion coefficient depends on an apparent bulk diffusivity evaluated using the Stokes−Einstein equation.

Theoretical Background. The permeate volume flux density is described by the Kedem-Katchalsky equation[36]

$$J_v = -L_p(\Delta P - \sigma_0 \Delta\pi) \tag{1}$$

where L_p is the membrane permeability, ΔP is the transmembrane pressure, $\Delta\pi$ is the difference in osmotic pressure, and σ_0 is the reflection coefficient. For dilute solutions, such as the ones studied here, the expression for the solute flux density reduces to

$$J_v = -L_p \Delta P = \frac{{r_p}^2}{8\mu l_{eff}} \Delta P \tag{2}$$

In this equation r_p is the effective membrane pore radius, μ is the dynamic viscosity of the solution in the membrane pores (considered to be equal to that of the bulk solvent), and l_{eff} is the effective membrane thickness associated with the permeate volume flux density. Equation 2 shows that the temperature can influence the permeate volume flux density via its effect on both the viscosity and the intrinsic membrane properties (r_p and l_{eff}).

According to the hindered transport theory for neutral solutes in cylindrical pores,[17,36] the rejection of solute i can be written in the form

$$R_i = 1 - \frac{c_{i,p}}{c_{i,a}} = \frac{\sigma_i(1-F)}{1-\sigma_i F} \tag{3}$$

with

$$F = \exp(-Pe) \tag{4}$$

and the Péclet number

$$Pe = J_v {l_{eff}}^i \frac{1-\sigma_i}{\Phi_i K_{i,d} D_i} \tag{5}$$

D_i is the solute bulk diffusion coefficient, related to the solute radius via the Stokes−Einstein equation:

$$D_i = \frac{k_B T}{6\pi\mu r_{i,s}} \tag{6}$$

Φ_i is the partition coefficient of solute i between the external solutions and the pore interior

$$\Phi_i = \left(1 - \frac{r_{i,s}}{r_p}\right)^2 \tag{7}$$

for $r_{i,s} < r_p$ ($R_i = 1$ for $r_{i,s} \geq r_p$). The reflection coefficient σ_i is given by

$$\sigma_i = 1 - K_{i,c}\Phi_i \tag{8}$$

$K_{i,d}$ and $K_{i,c}$ represent the diffusive and convective hindered transport coefficients calculated using the approximate formulas established by Bungay and Brenner.[18,36]

The rejection is an increasing function of the Péclet number. For high Péclet numbers, it tends toward a limiting value that is a function of the ratio of the solute Stokes radius to the membrane pore radius:

$$R_{i,lim} = \sigma_i = f\left(\frac{r_{i,s}}{r_p}\right) \tag{9}$$

Before reaching this limit, however, the rejection is also a function of l_{eff} and starts by increasing linearly with Pe.

$$R_i = \frac{\sigma_i Pe}{1-\sigma_i} = f\left(\frac{r_{i,s}}{r_p}, {l_{eff}}^i\right) \tag{10}$$

Equations 3−8 show that the effect of temperature T on the rejection of solute i can arise from a number of model parameters, including external ones such as the solute diffusion coefficient that depend explicitly and implicitly (via μ) on T and intrinsic ones

(32) Liu, T.; Ozisik, R.; Siegel, R. W. *J. Polym. Sci., Part B: Polym. Phys.* **2006**, *44*, 3546–3552.

(33) Kozlov, G. V.; Zaikov, G. E. *Structure of the Polymer Amorphous State*; Brill Academic Publishers: Utrecht, The Netherlands, 2004.

(34) Roguet, E.; Tence-Girault, S.; Tagnet, S.; Grandidier, J. C.; Hochstetter, G. *J. Polym. Sci., Part B: Polym. Phys.* **2007**, *45*, 3046–3059.

(35) Tang, C. Y.; Kwon, Y.-N.; Leckie, J. O. *Desalination* **2009**, *242*, 168–182.

(36) Chmiel, H.; Lefebvre, X.; Mavrov, V.; Noronha, M.; Palmeri, J. In *Handbook of Theoretical and Computational Nanotechnology*; Rieth, M., Schommers,W., Eds.; American Scientific Publishers: Stevenson Ranch, CA, 2006; Vol. *5*, pp 93−214.

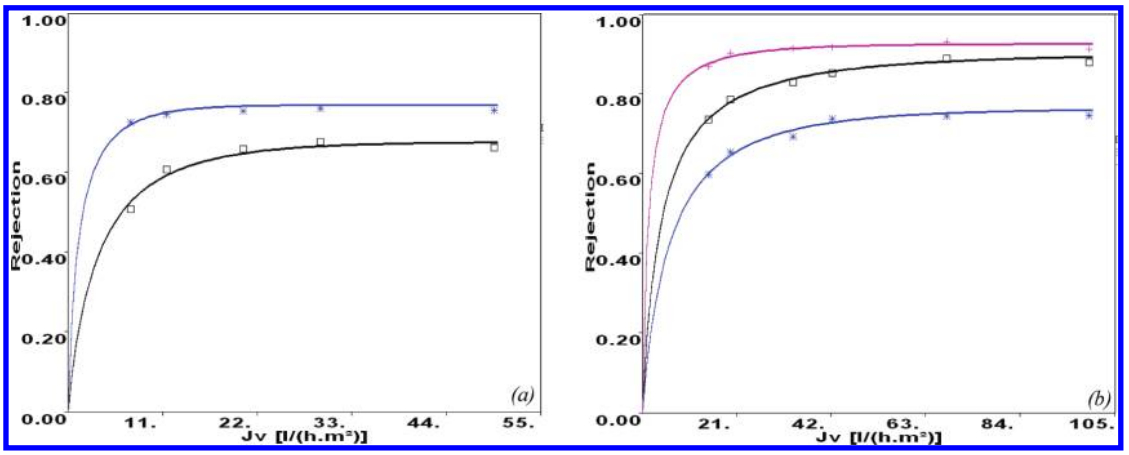

Figure 9. Rejection vs J_v in order of increasing rejection : model fit at 30 °C: (a) rejection of arabinose and glucose for the DK membrane and (b) rejection of ethylene glycol, glycerol, and diethylene glycol for the NF90 membrane.

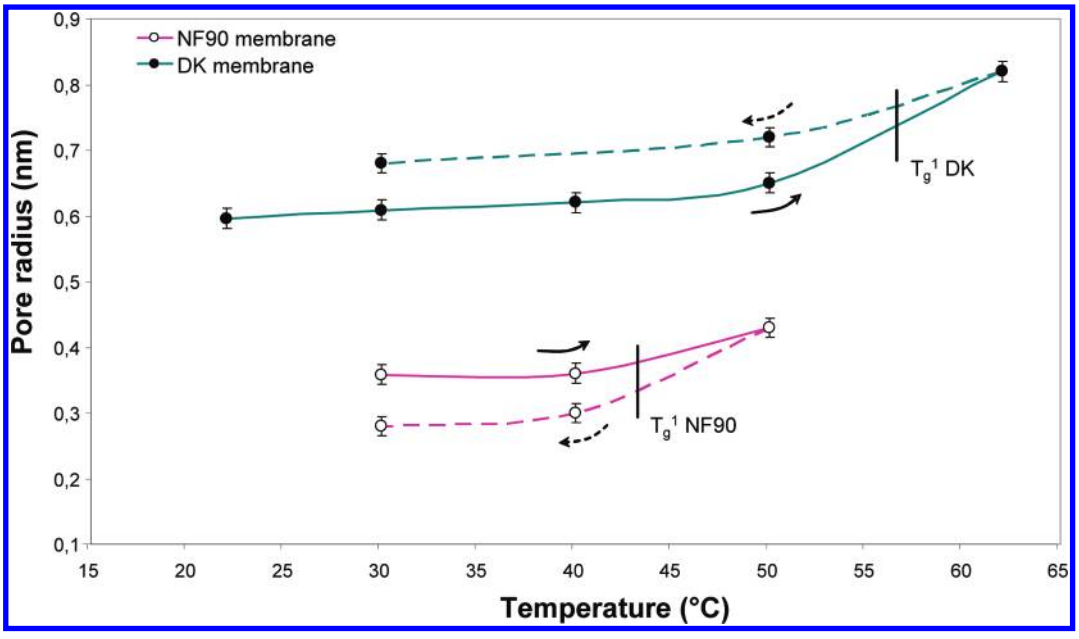

Figure 10. Evolution of the pore radius (r_p) of NF90 and DK membranes with temperature during the temperature cycle: upward (→) and downward (←---) directions.

such as σ_i, Φ_i, $K_{i,d}$, and $K_{i,c}$ following possible temperature-related structural modifications of the membrane (effective pore radius r_p and thickness l_{eff}).

Application of the Model. The variation of the intrapore viscosity is taken into account, assuming that it is directly proportional to the bulk viscosity. Modeling of the rejection (R) for uncharged solute as a function of the permeate volume flux (J_v) using the computer simulation program Nanoflux requires the adjustment of only two parameters: the effective pore radius and the effective membrane thickness. Thus, fitting the model to the experimental data allows us to estimate the effective membrane pore radius at a given temperature. In Figure 9a,b, we show, for example, the simulated rejection curves (solid lines) obtained by fitting the model to the experimental rejection for various solutes at 30 °C by the DK and NF90 membranes, respectively. The excellent agreement observed between the model fit and the data gives a unique effective pore radius value in each case with a standard deviation of about 0.03 nm.[11]

The fitted pore size versus the temperature reached during the temperature cycle experiment is plotted in Figure 10 for the two studied membranes. In the case of the DK membrane, no significant variation can be seen over the temperature range of 20−40 °C. However, approaching T_g^1 provokes a rapid increase in pore size. In the same way as for the rejection of uncharged solutes, no hysteresis takes place if the operating temperature remains below this value and the initial pore size value is recovered by decreasing the temperature. Going beyond T_g^1 results in an even greater increase in the pore radius that largely exceeds the standard deviation. Actually, it should be noted that the pore size variation from 22 to 60 °C is in the range of about 0.2 nm, a dramatic variation for an NF membrane. As expected from pure water permeability and neutral solute rejection data, hysteresis of the pore size is seen after decreasing the temperature to 30 °C in the second series of cycling experiments. Although the variation compared to the initial value is reduced, it still remains higher than 0.1 nm. However, the NF90 membrane shows an increase in pore radius similar to that of the DK by increasing the operating temperature even if the variation takes place to a much lesser extent (likely because of the more limited temperature domain studied). But the opposite trend is observed in this case

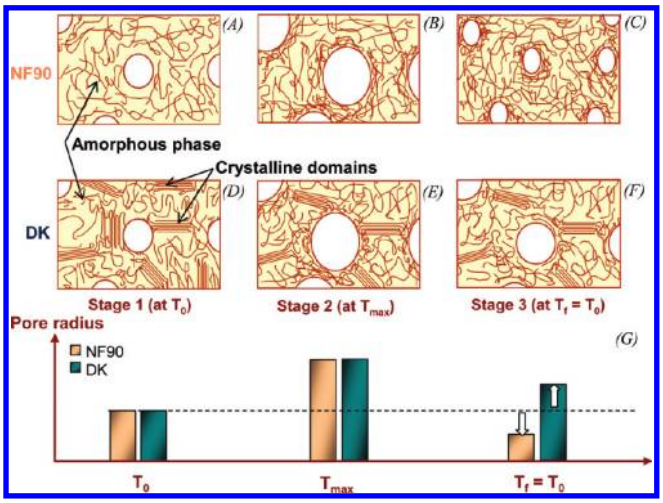

Figure 11. Schematic representation of the proposed deformation mechanism for the polymer constituting the active layer in three stages: (A, B, C) NF90 membrane, (D, E, F) DK membrane, and (G) variation of the pore radius for both membranes at each stage.

when the temperature is decreased to 30 °C for a cycle with T_{max} higher than T_g[1], which is evidenced by a significant decrease in the pore size compared to the initial value.

Proposed Mechanism of Deformation. Our findings demonstrated that the TAL of NF membranes undergoes structural changes upon increasing the temperature of feed solutions. The changes are reversible if the operating temperature remains below T_g and become irreversible in the opposite case. However, two different behaviors were observed depending on the presence of a crystalline phase in the TAL membrane. All of these data prove that the transition temperatures of the TAL play a key role in the control of NF membrane performance. We made the hypothesis that the observed pore deformation can probably be understood only by a combined effect of temperature and applied pressure. To verify this, we carried out the same experiment (temperature cycle with $T_{max} > T_g$[1]) but by applying a transmembrane pressure of only 1 bar. Under these conditions, the initial performance was recovered for NF membranes illustrating that irreversible deformation can take place only by a combination of high operating temperature and pressure.

On the basis of our results, we can now propose a deformation mechanism for the polymer constituting the TAL. The evolution of pore size is schematically represented for both membranes in Figure 11 at T_0, T_{max}, and T_f (equal to T_0) during a temperature cycle with T_{max} higher than T_g[1]. For the sake of clarity, membrane pores are represented in the initial stage by circles of the same size that are evenly distributed along the polymer matrix. In the case of the DK membrane, the polymer matrix contains a certain proportion of crystalline domains.

For operating temperatures below T_g[1] (Figure 11A,D), no significant deformation can take place owing to the rigid vitreous state of the amorphous phase accounting for the small and reversible change in the pore size. In the second stage, the operating temperature is now higher than T_g[1] (Figure 11B,E) and the amorphous phase enters the rubber state. It was proven that the combined effect of temperature and applied pressure during the filtration experiment enables the pore size to expand to a large extent because of the elasticity of the rubber state. During this stage, the polymer matrix is supposed to become more compact around the pores, forming a dense network.

The next stage, consisting of a decrease in temperature, induces the thermal contraction of the TAL resulting in a decrease in pore size. The following mechanism is proposed to explain the pore restriction observed in the case of the NF90 membrane (Figure 11C,G). The compacted network relaxes and pushes on the pore wall, giving rise to a pore size even smaller than that existing in the initial stage. The difference between the NF90 and DK TAL membranes lies in the presence of crystallites that are known to act as physical cross-linkers of the amorphous phase. On the basis of the evidence that we have presented here, we proposed that the crystalline domains are at the origin of the observed opposite variation of pore size by opposing the thermal contraction. This mechanism is expected to induce only a small decrease in pore size upon cooling. Therefore, for the DK membrane the final pore size is larger than the initial one because the increase in going from T_0 to T_{max} is less than the decrease in going from T_{max} to T_f. In this way, it is possible to understand how the NF90 and DK membranes can exhibit such opposite behavior when the operating temperature exceeds T_g[1].

Conclusions

Increasing the operating temperature strongly affects the transport properties of NF membranes through two significant effects: an enhancement of the permeate volume flux density and a decrease of the neutral solute rejection. These effects mainly originate from a decrease in the solvent intrapore viscosity for the former and from an increase in the pore size due to thermal expansion for the latter. These variations are reversible, meaning that the initial membrane performance is restored by decreasing the temperature back to the initial value provided that the maximum operating temperature remains lower than a certain critical temperature. We showed that the critical temperature value is directly related to the T_g of the corresponding TAL membrane. Beyond this critical value, TAL undergoes irreversible temperature-induced deformation by successive thermal expansion and contraction, which makes a reliable prediction of NF membrane transport properties difficult. Interestingly, two opposite variations in pore size were uncovered depending on the physical polymer state (amorphous or semicrystalline) in the TAL. The combined action of pressure and temperature was proven to be at the origin of the observed deformation, and a mechanism was proposed to explain it.

From our work, we can then conclude that the TAL T_g value is the limiting parameter for NF membrane applications at high temperature. Intriguingly, the T_g of an NF TAL membrane was found to be in the range of 40−50 °C whereas values higher than 100 °C were expected from their aromatic polyamide chemical nature. We assume that the low T_g observed in the case of the NF TAL membrane comes from the confinement of the polymer network to a very thin layer, resulting in a dramatic decrease in its T_g value. It then appears that the enhancement of the TAL T_g is not a trivial matter and a significant improvement in high-temperature NF membrane performance could be achieved by solving this problem.

Note Added after ASAP Publication. This article was published ASAP on October 7, 2009. Several reference changes have been made in the manuscript. The correct version was published on October 16, 2009.

Acknowledgment. We thank the French Ministry of Foreign Affairs for partial funding (CMCU project 04PRE01). We also thank Didier Cot and Nathalie Masquelez for their

technical assistance in SEM observations and DSC experiments, respectively.

Glossary

T_g	glass-transition temperature
T_{max}	maximum temperature in each cycle
T_m	melting point
NF	nanofiltration
PA	polyamide
PS	polysulfone
TAL	thin active layer
c_m, c_p	membrane surface concentration, permeate concentration, M
D_i	bulk solute diffusivity, $m^2\ s^{-1}$
J_v^w, J_v	water, solution, volume flux density, L/(h m^2)
L_p	membrane permeability, L/(h m^2 bar)
L^i_{eff}	effective thickness of the membrane seen by the solute i, μm
Pe_s	Peclet number
R^i	rejection coefficient of the solute i
R^i_{lim}	highest rejection coefficient
r_i	solute radius, nm
r_p	pore radius, nm
T	temperature, °C
K_c, K_d	hindered transport factors
ΔP	mean transmembrane pressure, bar
$\Delta\pi$	osmotic pressure difference across the membrane, bar
Φ_{ic}	solute partition coefficient
Φ_{steri}	solute steric partition coefficient
μ	dynamic water viscosity, Pa·s
σ_s	filtration reflection coefficient